EFFECTS OF PLASTICITY AND STRAIN RATE ON FATIGUE CRACK GROWTH

L.Guerra Rosa*, C.M.Branco** and J.C.Radon***

A general relationship for the calculation of strain rates at a fatigue crack tip was derived and used to predict the effect of strain rate on the yield stress of metallic materials and consequently on the dimensions of the monotonic and cyclic plastic zones. Plastic zones were measured in a medium strength ferrite-pearlite steel (BM45) fatigue tested at 25 Hz at room temperature. Two methods were applied: microhardness and the "fatigue in compression" technique. The retardation effects due to overloads were analysed using the da/dN vs. ΔK relationship. Finally it is suggested that in ductile metals a steady state of fatigue crack growth occurs under plane strain conditions.

INTRODUCTION

The prediction of fatigue crack propagation at cyclic peak loads is usually based only on the size of the plastic zone. However recent studies show that the shape of the plastic zone may influence not only the growth rate of a fatigue crack but also its direction.

Since the dimension of the plastic zone at any θ-angle, r_p^θ, depends on the applied K and on σ_{ys} according to the equation,

$$r_p^\theta = \alpha^\theta \left(\frac{K_{max}}{\sigma_{ys}} \right)^2 \qquad \text{Eq.(1)}$$

only the values of the constant α^θ are of interest (1).

In the simplest case of constant-amplitude fatigue, a cyclic plastic zone, as well as a monotonic plastic zone, will be created. Theoretically, ignoring the effect of strain hardening, strain ageing and strain rate, the dimensions of this cyclic plastic zone, r_c^θ, will be one quarter of the r_p^θ-values i.e. $\alpha^\theta/\alpha_c^\theta = 4$.

For the correct evaluation of plastic zone dimensions the well-known effect of strain rate on the yield stress of metallic materials must also be taken into account. In many studies the strain rate effect has been omitted. In this paper some properties of the monotonic and cyclic plastic zones are investigated and the influence of the high strain rates occuring at the fatigue crack tip on the plastic behaviour of the material discussed.

*CEMUL-Instituto Superior Técnico, 1096 Lisboa Codex, Portugal
**Universidade do Minho, Braga, Portugal
***Department of Mechanical Engineering, Imperial College, London, UK

EXPERIMENTAL TECHNIQUES

Material: Composition and Properties

The material investigated in this study was the medium strength steel BM45 (Ck45 according to DIN 17200) widely used as a structural steel in machine components. The chemical composition was C-0.45%; Mn-0.74%; Si-0.20%; Ni-0.06%; P-0.027%; S-0.027%; Cr<0.03%. The mechanical properties in the as-received condition corresponding to a normalized ferritic-pearlitic microstructure with an average grain size of 9.2 μm were: σ_{ys}(0.2% yield stress)=335 MN m^{-2}; σ_{UTS} (ultimate tensile strength)=640 MN m^{-2}; ε_{max}(engineering strain at σ_{UTS})=16.5% and E=2.07 x 10^5 MN m^{-2}.

Fatigue Tests

Fatigue crack propagation tests were conducted according to ASTM Method E647-78T using compact type (CT) specimens. The specimen dimensions were: width, W=55 mm and thickness,B=6 mm. Tests were performed in air at room temperature, at a frequency of 25 Hz with the stress ratio R=0.1 applying a sinusoidal load in a load controlled closed loop hydraulic fatigue machine MTS,type 811.02 . The crack length was monitored with a low power (30x) travelling microscope fitted with a dial gauge with an accuracy of 0.02 mm.

Microhardness Measurements for the Plastic Zone

Microhardness measurements were performed using a Reichert Microhärteprüfer instrument on the polished surface of one fatigue specimen. For maximum resolution each indentation was made within one ferrite grain. The measurements were made at various distances in a direction normal to the crack plane and were restricted to the zone in which the fatigue crack was still closed. The applied K_{max} was 51.8 MN $m^{-3/2}$ ± 3%. The indentations were positioned at 50 and 100 μm-intervals on both sides of the crack plane.

In order to assess the reliability and accuracy of the microhardness technique a calibration curve HV_{20g} as a function of the true stress $\bar{\sigma}$ was obtained. These microhardness measurements were made on the larger ferrite grains of tensile specimens split longitudinally in halves.

Fatigue In Compression

In this technique,originally described by Reid et al (2),a plastic zone was created by a suitable monotonic compressive load L_1. The CT specimen was then subjected to a cyclic compressive load varying between 0 and L_2 where $|L_2|<|L_1|$ with the consequent nucleation and growth of a fatigue crack from the original notch tip. This fatigue crack grows due to the reversals of tensile stresses existing within the plastic zone. It is obvious that the crack will stop on reaching the boundary of the plastic zone corresponding to the previously applied compressive load L_1 and the relevant value of the stress intensity K.

RESULTS AND DISCUSSION

Experimental α^θ and α_c^θ Measurements

In order to determine the respective plastic zone sizes Fig.1 shows the microhardness measurements obtained on the surface of one fatigue specimen 6 mm thick. Only the cyclic plastic zone boundary can be identified because this technique is not sufficiently accurate for stress values near σ_{ys} as can be seen from the calibration curve shown in Fig.2.

Tests using the "fatigue in compression" method were performed on CT specimens of three different thicknesses,B = 5.95, 19.3 and 24.2 mm. All notch tips were machined using a jewellery saw with 0.2 mm blade thickness.

TABLE 1 - Experimental α^{θ} and α_c^{θ}-measurements in the BM45 steel under Pσ conditions.

With the "microhardness" technique: $\alpha_c^{90^0} = 0.012-0.013$

With the "fatigue in compression" technique:

Specimen	Spec.Thickness B (mm)	Compressive K_{max} (MN $m^{-3/2}$)	$r_p^{0^0}$ (mm)	α^{0^0}
CT-X1	5.95	66.64	7.40	0.187
CT-A	19.30	55.62	5.10	0.185
CT-D	24.20	54.20	5.00	0.191
			α^{0^0} (mean value) =	0.188

Table 1 summarizes the α^{0^0} and $\alpha_c^{90^0}$-values obtained by $r_p^{0^0}$ and $r_c^{90^0}$--measurements. These results can be compared with other experimental values available in the literature (2-14). The plane stress (Pσ) data were obtained from measurements on the specimen surface and the plane strain (Pε) results derived from measurements at the interior when a high degree of plane strain was expected. The analysis of these results shows a large scatter in the values of $\alpha^{\theta}/\alpha_c^{\theta}$ ratio measured at the specimen surface. The ratios $\alpha^{\theta}/\alpha_c^{\theta}$ differ greatly from the theoretical value of 4 (values between 7.8% and 24.0% have been reported). Monotonic plastic zones at the surface (Pσ) show α^{0^0} and α^{90^0} values varying between 0.1 and 0.2. Contrary to Pσ cases the scatter in the $\alpha^{\theta}/\alpha_c^{\theta}$ values in Pε is considerably reduced with all the ratios being higher than 4 (between 4.0 and 5.6) and an average ratio of approximately 5. For Pε the α^{0^0} values range between 0.03 and 0.08 and the α^{90^0} vary between 0.04 and 0.1 with an average of 0.05.

It is assumed that the large scatter found in the $\alpha^{\theta}/\alpha_c^{\theta}$-ratio measured at the specimen surface is a result of considering both α^{θ} and α_c^{θ}-values under the same state of stress. In reality, the average experimental $\alpha_c^{0^0}$ and $\alpha_c^{90^0}$-values in Pσ are respectively 0.008 and 0.012. The corresponding values in Pε are 0.012 and 0.013. In spite of the very few data for $\alpha_c^{0^0}$ it may be concluded that all the α_c^{θ}-values correspond to plane strain (Pε) states. This argument may be reinforced by the experimental evidence showing that in ductile metals the steady state of fatigue crack growth generally follows a transgranular striation mechanism. This type of mechanism and striation orientation is not possible in a Pσ state because in this state and for $\theta=0^0$ ($\sigma_1=\sigma_{ys}$ and $\sigma_3=\sigma_z=0$) the maximum (macroscopic) shear stress τ_{max} occurs in planes passing through the X axis and making 45^0 with σ_1 (Y direction) and σ_3 (Z direction) as indicated in Fig.3. On the other hand, in Pε both the same mechanism and the resulting striation orientation are possible. In this case σ_1 and σ_2 have the same magnitude as in Pσ and $\sigma_3=\nu(\sigma_1+\sigma_2)$. In Pε and as also shown in Fig.3, the maximum shear stress occurs for planes passing through the Z axis and making 45^0 with σ_1 (Y direction) and σ_2 (X direction).

The Effect of Overloads

A typical fatigue crack propagation test was performed using one CT specimen. The crack length vs.number of cycles is shown in Fig.4. This test was conducted until a crack length of a=17.84 mm was reached. At the point P_1 a single overload of 19600 N (K=85.10 MN $m^{-3/2}$) was applied. The fatigue test was then restarted and when the crack length reached 19.61 mm (P_2 in Fig.4) another peak load of 9800 N (K=46.25 MN $m^{-3/2}$) was applied by the same technique. Subsequently the fatigue test was continued up to a=34.20 mm.

Based on the experimental α^{0^0}-value previously measured with the "fatigue in compression" technique, it is possible to estimate the extent of the monotonic plastic zones corresponding to each peak load. Therefore, assuming a Pσ condition α^{0^0}=0.188, for the 19600 N peak load: $r_p^{0^0}$ (centered at P_1)=12.13 mm and for the 9800 N peak load: $r_p^{0^0}$ (centered at P_2)=3.58 mm. Thus, the monotonic zone created by the 19600 N peak load at a=17.84 mm extended as far as a=29.97 mm; the monotonic zone corresponding to 9800 N (at a=19.61 mm) had its boundary at a=23.19 mm. This means that the monotonic zone for the second overload was contained within the monotonic zone for the first overload.

Figures 4 and 5 show that the retardation effect appeared after the first overload. Similarly another decrease in crack propagation rate occured due to the second overload. In spite of an increasing ΔK field some crack growth rates measured after P_2 were lower than the observed da/dN-values between P_1 and P_2. It is clear that the residual compressive stresses within the second overload zone were higher than those existing within the first overload zone. The effect of this second overload was to decrease again the effective ΔK at the crack tip, ΔK_{eff}.

The usual da/dN vs. ΔK plot (R=0.1) for constant-amplitude fatigue test is also presented in Fig.5 (solid line). This plot was obtained by fitting a curve to the results of tests conducted on three identical CT specimens. It can be concluded that the retardation effect due to overloading fully disappeared when ΔK in that test was approximately 55 MN $m^{-3/2}$ which corresponds to a crack length a=30.6 mm. This result confirms the previously computed value of the overall plastic zone boundary (a=29.97 mm).

Strain Rate Effects

Theoretical Calculations of $\dot{\varepsilon}$ at the Monotonic and Cyclic Plastic Zone Boundaries. It is known that Pε conditions are very important in fracture studies. Therefore it is worth obtaining the values of $\dot{\varepsilon}$ at both the monotonic and the cyclic plastic zone boundaries (boundaries 1 and 2 shown in Fig.6) and analysing the strain rate effects.

Based on a previous analysis of Hahn and Rosenfield (15), the tensile strain at boundary 1, ε_1, for Pε conditions is:

$$\varepsilon_1 \simeq \frac{K_{max}^2}{2\, r_p^{0^0}\, E\, \sigma_{ys}} \qquad \text{Eq.(2)}$$

Therefore the strain rate is:

$$\dot{\varepsilon}_1 \simeq \frac{K_{max}}{r_p^{0^0}\, E\, \sigma_{ys}}\, \dot{K} \qquad \text{Eq.(3)}$$

where $\dot{K}$ is the rate of change of the stress intensity factor with time.

Using the experimental α^{0^0}-value of 0.05 for boundary 1 in Pε conditions, $r_p^{0^0}$ is given by Eq.(1). Substituting $r_p^{0^0}$ in Eq.(3) we obtain:

$$\dot{\varepsilon}_1 \simeq \frac{20\, \sigma_{ys}}{E}\, \frac{\dot{K}}{K_{max}} \qquad \text{Eq.(4)}$$

In constant-amplitude fatigue with sinusoidal loading the average value of $\dot{K}$ is approximately $(K_{max}-K_{min})/t$ or $\dot{K} = K_{max}(1-R)/t$, where $t=(2f)^{-1}$ is the half

cycle period. Hence Eq.(4) becomes:

$$\dot{\varepsilon}_1 \simeq 40(1-R)\,\frac{\sigma_{ys}}{E}\,.\,f \qquad \text{Eq.(5)}$$

This equation implies that $\dot{\varepsilon}_1$ is independent of the applied K_{max} for a steady state of cyclic crack growth, but varies with the test conditions, such as frequency and the stress ratio R, and with the material parameters σ_{ys} and E.

For the boundary 2 Eq.(3) may also be used substituting $r_p^{0^0}$ by $r_c^{0^0}$. Considering $r_c^{0^0} = r_p^{0^0}/4$, the strain rate at the cyclic boundary will be:

$$\dot{\varepsilon}_2 = 4\,\dot{\varepsilon}_1 \qquad \text{Eq.(6)}$$

Plastic Zone Size Corrections Due to Strain Rate Effects. In the previous equations the static yield stress σ_{ys} was used. But, since the real yield stress of the material depends on temperature and strain rate, it is more appropriate to use the proper dynamic yield stress for each temperature and cyclic frequency. At room temperature, the appropriate equations for $r_p^{0^0}$ and $r_c^{0^0}$ are:

$$r_p^{0^0} = \alpha'\left(\frac{K_{max}}{\sigma_{ys}^{d_1}}\right)^2 \qquad r_c^{0^0} = \alpha'\left(\frac{K_{max}}{\sigma_{ys}^{cd2}}\right)^2 \qquad \text{Eqs.(7)}$$

where α' is a constant, σ_{ys}^{d1} is the dynamic yield stress at boundary 1 and σ_{ys}^{cd2} is the cyclic-dynamic yield stress at boundary 2. The cyclic-dynamic yield stress can be estimated as: $\sigma_{ys}^{cd2} = 2\,\sigma_{ys}^{d2}$; σ_{ys}^{d2} being the dynamic yield stress at boundary 2.

For the 25 Hz fatigue tests (R=0.1) in the BM45 steel at room temperature, using Eqs.(5) and (6) the following values of $\dot{\varepsilon}$ are obtained: $\dot{\varepsilon}_1 \simeq 1.5\ \text{sec}^{-1}$ and $\dot{\varepsilon}_2 \simeq 6\ \text{sec}^{-1}$. Correcting now for the dynamic yield stresses using experimental data for similar steels (16-19) it is found that $\sigma_{ys}^{d1} = 1.20\,\sigma_{ys}$ and $\sigma_{ys}^{d2} = 1.30\,\sigma_{ys}$.

Hence Eqs.(7) can be set out in the same way as Eq.(1):

$$r_p^{0^0} = \frac{\alpha'}{(1.20)^2}\left(\frac{K_{max}}{\sigma_{ys}}\right)^2 \qquad r_c^{0^0} = \frac{\alpha'}{(2\text{x}1.30)^2}\left(\frac{K_{max}}{\sigma_{ys}}\right)^2$$

and the theoretical $\alpha^{0^0}/\alpha_c^{0^0}$-ratio will be:

$$\frac{\alpha^{0^0}}{\alpha_c^{0^0}} = \frac{\alpha'/(1.20)^2}{\alpha'/(2\text{x}1.30)^2} = 4.7$$

This value of 4.7, for a theoretical $\alpha^{0^0}/\alpha_c^{0^0}$-ratio applicable to fatigue crack propagation tests at 25 Hz (R=0.1) in the BM45 steel shows that, taking into account the strain rate effects, a theoretical $\alpha^{\theta}/\alpha_c^{\theta}$-ratio higher than 4 is always found and may explain the experimental $\alpha^{\theta}/\alpha_c^{\theta}$ values (in Pε) reported in the literature.

CONCLUSIONS

I. The "microhardness" technique is not sufficiently accurate to obtain monotonic plastic zone sizes in a ferrite-pearlite steel with a small grain size. However this technique when used properly enables the determination of the cyclic plastic zone in a direction normal to the fracture plane, $r_c^{0^0}$

II. The "fatigue in compression" technique permits a very accurate determination of monotonic zone sizes in the $\theta=0^0$ direction.

III. An analysis of experimental results available in the literature showed a good agreement among the values of α_c^θ, coefficient for the cyclic plastic zone size. Taking into account this evidence and the plasticity criteria for the striation mechanism it may be suggested that in the steady state fatigue of ductile metals, the cyclic zone is generated under plane strain conditions.

IV. The introduction of single and periodic overloads into constant-amplitude fatigue tests confirmed the existence of delayed retardation.

V. The correct theoretical formulae for both cyclic and monotonic plastic zone dimensions should include the proper dynamic yield stresses. This difficulty may be overcome using the experimental α_c^θ and α^θ-values. The values of experimental $\alpha^\theta/\alpha_c^\theta$ - ratios higher than 4 for PE conditions may be explained by the high strain rates usually occuring at the fatigue crack tip.

ACKNOWLEDGEMENT

The experimental facilities provided by Departamento de Metalurgia e Metalomecânica of L.N.E.T.I. (Sacavém - Portugal) are gratefully acknowledged.

REFERENCES

1. Guerra Rosa,L.,and Branco,C.M.,1980 "A Mecânica da Fractura e a Fadiga com Corrosão:Parte III",Relatório Interno CEMUL,Lisboa.
2. Reid,C.N.,Williams,K.,and Hermann,R.,1979,Fatigue Engng Mater.Struct.,1, pp.267-270.
3. Hahn,G.T.,Hoagland,R.G.,and Rosenfield,A.R.,1972,Met.Trans.3,pp.1189-1202.
4. Davidson,D.L.,Lankford,J.,Yokobori,T.,and Sato,K.,1976,Eng.Fract.Mech.12, pp.579-585.
5. Yokobori,T.,Sato,K.,and Yaguchi,H.,1973 "Reports of the Research Institute for Strength and Fracture of Materials",Tohoku University,Sendai,Japan,Vol. 9,1,pp.1-10.
6. Davidson,D.L.,and Lankford,J.,1976,J.Engng.Mat.Tech.98,pp.17-29.
7. Bathias,C.,and Pelloux,R.M.,1973,Met.Trans.4,pp.1265-1273.
8. Pineau,A.G.,and Pelloux,R.M.,1974,Met.Trans.5,pp.1103-1112.
9. Clavel,M.,Fournier,D.,and Pineau,A.G.,1975,Met.Trans.6A,pp.2305-2307.
10. Wilkins,M.A.,and Smith,G.C.,1970,Acta Met.18,pp.1035-1043.
11. Davidson,D.L.,and Lankford,J.,1980,Fatigue Engng Mater.Struct.,3,pp.289-303.
12. Saxena,A.,and Antolovich,S.D.,1975,Met.Trans.6A,pp.1809-1828.
13. Lankford,J.,Davidson,D.L.,and Cook,T.S.,1977 "Fatigue Crack Tip Plasticity", ASTM STP 637,pp.36-55.
14. Wanhill,R.J.H.,1976,Met.Trans.7A,pp.1365-1373.
15. Hahn,G.T.,and Rosenfield,A.R.,1966,Trans.ASM,59,pp.909-919.
16. Rosenfield,A.R.,and Hahn,G.T.,1966,Trans.ASM,59,pp.962-980.
17. Kanninen,M.F.,Mukherjee,A.K.,Rosenfield,A.R.,and Hahn,G.T.,1967 "The Speed of Ductile Crack Propagation and the Dynamics of Flow in Metals",Symp. on Mech. Behaviour of Metals under Dynamic Loads,San Antonio,Texas.
18. Shoemaker,A.K.,and Rolfe,S.T.,1971,Eng.Fract.Mech.2,p.319.
19. Hertzberg,R.W.,1976 "Deformation and Fracture Mechanics of Engineering Materials",J.Wiley Sons,pp.35-37.

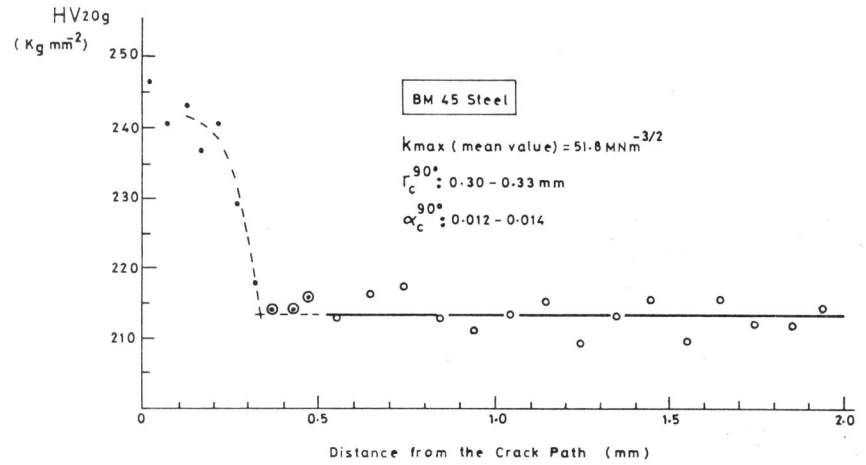

Figure 1. Cyclic plastic zone size determination by microhardness measurements at the specimen surface.

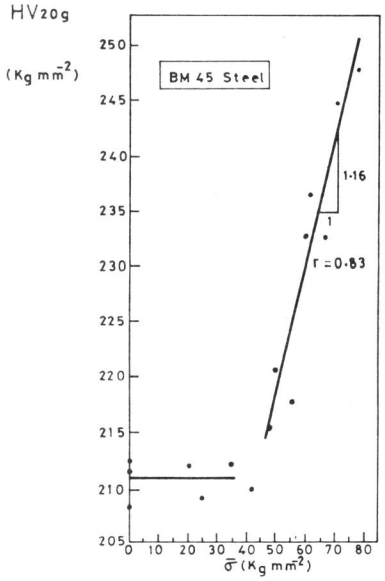

Fig.2 Variation of microhardness with true tensile stress(Calibration Curve)

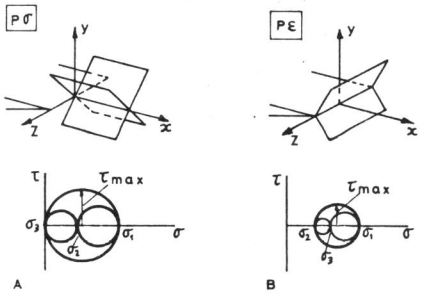

Fig.3 Planes of maximum shear stress for $\theta = 0^0$: A.Plane stress;B.Plane strain

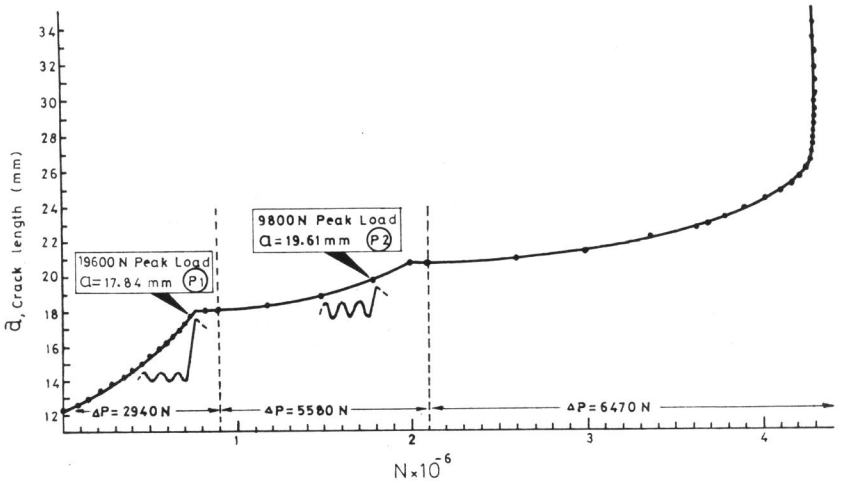

Figure 4. Crack length versus number of cycles N for constant amplitude loading with peak loads at points P1 and P2

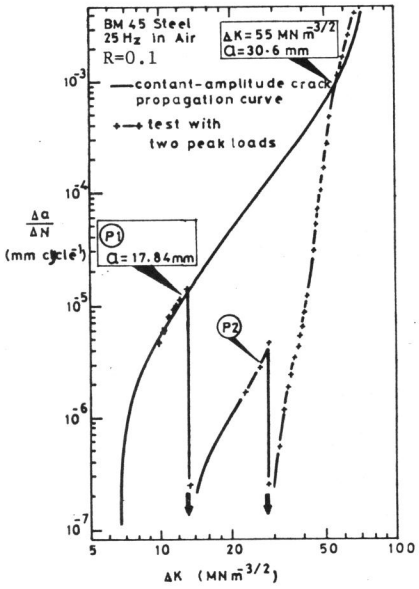

Fig.5 The $\Delta a/\Delta N$ - ΔK curves with and without overloading.

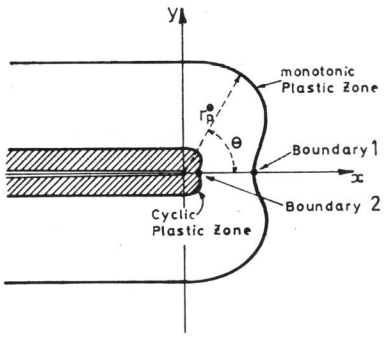

Fig.6 Schematic drawing of plastic zones around a fatigue crack in Pε.